

# Georgia Tech Catalog of Gravitational Waveforms

Karan Jani,<sup>1</sup> James Healy,<sup>2,1</sup> James A. Clark,<sup>1</sup> Lionel London,<sup>3,1</sup> Pablo Laguna,<sup>1</sup> and Deirdre Shoemaker<sup>1</sup>

<sup>1</sup>*Center for Relativistic Astrophysics and School of Physics*

*Georgia Institute of Technology, Atlanta, GA 30332*

<sup>2</sup>*Center for Computational Relativity and Gravitation*

*Rochester Institute of Technology, Rochester, NY 14623*

<sup>3</sup>*School of Physics and Astronomy, Cardiff University*

*Queens Building, CF24 3AA, Cardiff, United Kingdom*

This paper introduces a catalog of gravitational waveforms from the bank of simulations by the numerical relativity effort at Georgia Tech. Currently, the catalog consists of 452 distinct waveforms from more than 600 binary black hole simulations: 128 of the waveforms are from binaries with black hole spins aligned with the orbital angular momentum, and 324 are from precessing binary black hole systems. The waveforms from binaries with non-spinning black holes have mass-ratios  $q = m_1/m_2 \leq 15$ , and those with precessing, spinning black holes have  $q \leq 8$ . The waveforms expand a moderate number of orbits in the late inspiral, the burst during coalescence, and the ring-down of the final black hole. Examples of waveforms in the catalog matched against the widely used approximate models are presented. In addition, predictions of the mass and spin of the final black hole by phenomenological fits are tested against the results from the simulation bank. The role of the catalog in interpreting the GW150914 event and future massive binary black-hole search in LIGO is discussed. The Georgia Tech catalog is publicly available at [einstein.gatech.edu/catalog](http://einstein.gatech.edu/catalog).

PACS numbers: 04.25.D-, 04.25.dg, 04.30.Db, 04.80.Nn

## I. INTRODUCTION

Gravitational wave astronomy is finally here with the detection of transient GW150914 [1]. The detection was both a triumph and a surprise: a triumph because the Laser Interferometer Gravitational Wave Observatory (LIGO) [2] achieved unprecedented sensitivity, and a surprise because of the particular characteristics of the source. The GW150914 transient was identified [3] as the gravitational waves (GWs) produced by the merger of a binary black hole (BBH) at a distance of  $410^{+160}_{-180}$  Mpc. The masses of the black holes (BHs) were surprisingly large ( $m_1 = 36^{+5}_{-4} M_\odot$  and  $m_2 = 29^{+4}_{-4} M_\odot$ ,  $q = m_1/m_2 \approx 1.22$ ) with net spins canceling each other ( $\chi_{\text{eff}} \approx -0.06$ ). It is estimated that the coalescence left behind a rotating BH with a mass  $M_f = 62^{+4}_{-4} M_\odot$  and spin  $\chi_f = 0.67^{+0.05}_{-0.07}$ , thus suggesting that about  $3 M_\odot$  was emitted in GWs.

The role of numerical relativity (NR) simulations was evident in GW150914 event. The detection paper [1] showed the best fits of a NR waveform to the data. The papers on parameter estimation [3] and tests of general relativity [4] made it clear that results from BBH simulations were used to build the **SEOBNRv2** and **IMRPhenomPv2** waveform models used in the analysis. And directly relevant to the present work, the paper on the analysis of the GW150914 event with minimal assumptions [5] included results of matches using waveforms from the Georgia Tech (GT) catalog introduced in this paper.

The goal of this paper is to formally introduce the GT catalog of GW waveforms. Currently, the catalog consists of 452 distinct waveforms from a bank of more than 600 BBH simulations produced by the NR effort at GT. Among the 452 waveforms, 128 are from binary systems

with BHs non-precessing spins, i.e. no spins or spins such that they are parallel (aligned, or anti-aligned) with the orbital angular momentum  $\vec{L}$ ; and, 324 waveforms are from generic spin configuration that lead to precessing BBH systems (see Fig. 1). The catalog probes mass-ratios of  $q \leq 15$  for binaries with non-spinning BHs and  $q \leq 8$  for binaries with precessing, spinning holes. The waveforms cover a moderate number of GW cycles in the late inspiral, the merger of the binary, and ends with the ring-down of the final BH.

The waveforms are given in terms of an adjustable mass scale (the total mass  $M = m_1 + m_2$  of the BBH system); and, therefore, they can be rescaled for both ground and space-based GW detectors. In this paper, we focus the discussion on the relevance of the catalog to data analysis for ground detectors such as LIGO.

Within the sensitivity window of LIGO (10 – 1000 Hz) the waveforms in the catalog can be in general used in two ways. For binary systems with masses  $M \geq 60 M_\odot$ , as in GW150914, the binary system is observed for less than half a dozen GW cycles before merger. A substantial fraction of the waveforms in the GT catalog expand this dynamical range. They can thus be applied directly in analysis massive BBH mergers. On the other hand, for binary systems with  $M \leq 60 M_\odot$ , more cycles are needed for detection and parameter estimation [6–9]. Our catalog also includes waveforms with enough cycles to help improve Effective One Body Approach (EOB) [10] and IMR (Inspiral-Merger-Ringdown) [11] waveform models.

The paper is organized as follows: Section II provides a description of the NR code used to produce the catalog, namely the MAYA code. This Section also includes a discussion of the errors in phase and amplitude of the extracted GWs. Section III describes the parame-

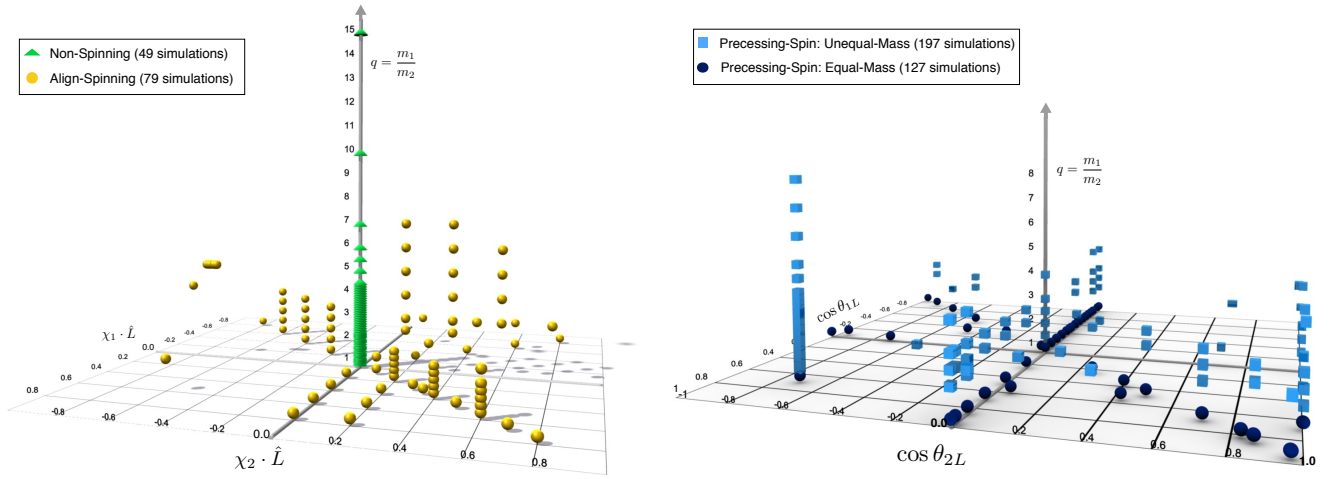


FIG. 1: Coverage of binary black hole parameter space by the GT catalog. The vertical axis in both plots denotes the mass ratio  $q$ . The plot on the left is for non-spinning and aligned-spin systems, and on the right for precessing binaries.

ter space and some of the key features of the GT catalog. Section IV compares a few of the waveforms in the catalog with the `SEOBNRv2` and `IMRPhenomPv2` waveform models. Section V compares the parameters of remnant BH, namely mass and spin, with the phenomenological fits [12–14]. Conclusions are given in Sec. VI.

## II. MAYA CODE AND ERROR ANALYSIS

All the BBH simulations in the GT catalog were obtained with our `MAYA` code [15–18]. The code is based on the BSSN formulation of the Einstein equations [19], and for BBH simulation it uses the moving puncture gauge condition [20, 21]. `MAYA` is very similar to the Einstein code in the `EINSTEINTOOLKIT` [22]. That is, it operates under the `CACTUS` infrastructure [23], with `CARPET` providing mesh refinements [24] and thorns (modules) generated by the package `KRANC` [25].

The initial data for each simulation consist of the extrinsic curvature and spatial metric. The extrinsic curvature has the Bowen-York [26] form, and the spatial metric is conformally flat. The conformal factor is obtained by solving the Hamiltonian constrain using the `TWOPUNCTURES` spectral solver [27]. The input parameters for each initial data set are: BH masses  $m_1, m_2$ , spins  $\vec{\chi}_1, \vec{\chi}_2$ , momenta  $\vec{P}_1, \vec{P}_2$ , and the binary separation  $r$ . A script that solves the post-Newtonian (PN) equations of motion for binaries in quasi-circular orbits [28, 29] is used to set the spins  $\vec{\chi}_1, \vec{\chi}_2$  and momenta  $\vec{P}_1, \vec{P}_2$  at the binary separation  $r$  in the initial data where the NR evolution will start. The mass and spin of the final BH are obtained from both its apparent horizon and quasi-normal ringing.

The GW waveforms are extracted from the simulation data via the Weyl Scalar  $\Psi_4$  [30]. The extraction is done in the source frame such that the initial orbital angular

momentum of the binary is pointing in the positive  $z$ -direction. We store  $\Psi_4$  decomposed into spin-weighted spherical harmonics as

$$RM \Psi_4(t; \Theta, \Phi) = \sum_{\ell, m} A_{\ell m}(t) e^{i\phi_{\ell m}(t)} {}_{-2}Y_{\ell m}(\Theta, \Phi), \quad (1)$$

with both  $A_{\ell m}$  and  $\phi_{\ell m}$  real functions of time,  $M$  the total mass of the binary, and  $R$  the extraction radius. Given  $\Psi_4$ , the GW strain polarizations  $h_+$  and  $h_\times$  are obtained from integrating  $\Psi_4 = \ddot{h}_+ - i\ddot{h}_\times \equiv \ddot{h}^*$ , with star denoting complex conjugation and over-dots time derivatives.

To give a general sense of the accuracy of the waveforms, we select two cases in the catalog: one with BH spins aligned with the orbital angular momentum and another with precessing BHs (GT0582 and GT0560 cases respectively in the catalog, see next Section). Fig. 2 summarizes the accumulated numerical errors in the GW strain,  $h(t)$ , from combined  $\ell = 2 : 6, m = -\ell : \ell$  radiated mode. The left panels show the results for the aligned-spinning case GT0582, and the right panels for the precessing-spin case GT0560. Top row panel depicts the strain  $h(t)$ . The middle and bottom panels show accumulated errors in phase and amplitude for each of the available resolutions, four resolutions for GT0582 and three for GT0560. For each resolution, the errors are computed against a waveform obtained from Richardson extrapolation to the continuum using the available resolutions.

Table I summarizes the errors in phase and amplitude are also reported for early inspiral and reference frequency  $M\omega = 0.2$  (near merger). The error-analysis is similar to the one reported in [31]. The mismatches are computed between two finite numerical grid resolutions and finite waveform extraction radius ( $R$  in Eq. 1). These match calculations involve advanced LIGO noise curve and total-mass of BBH scaled at  $100 M_\odot$ .

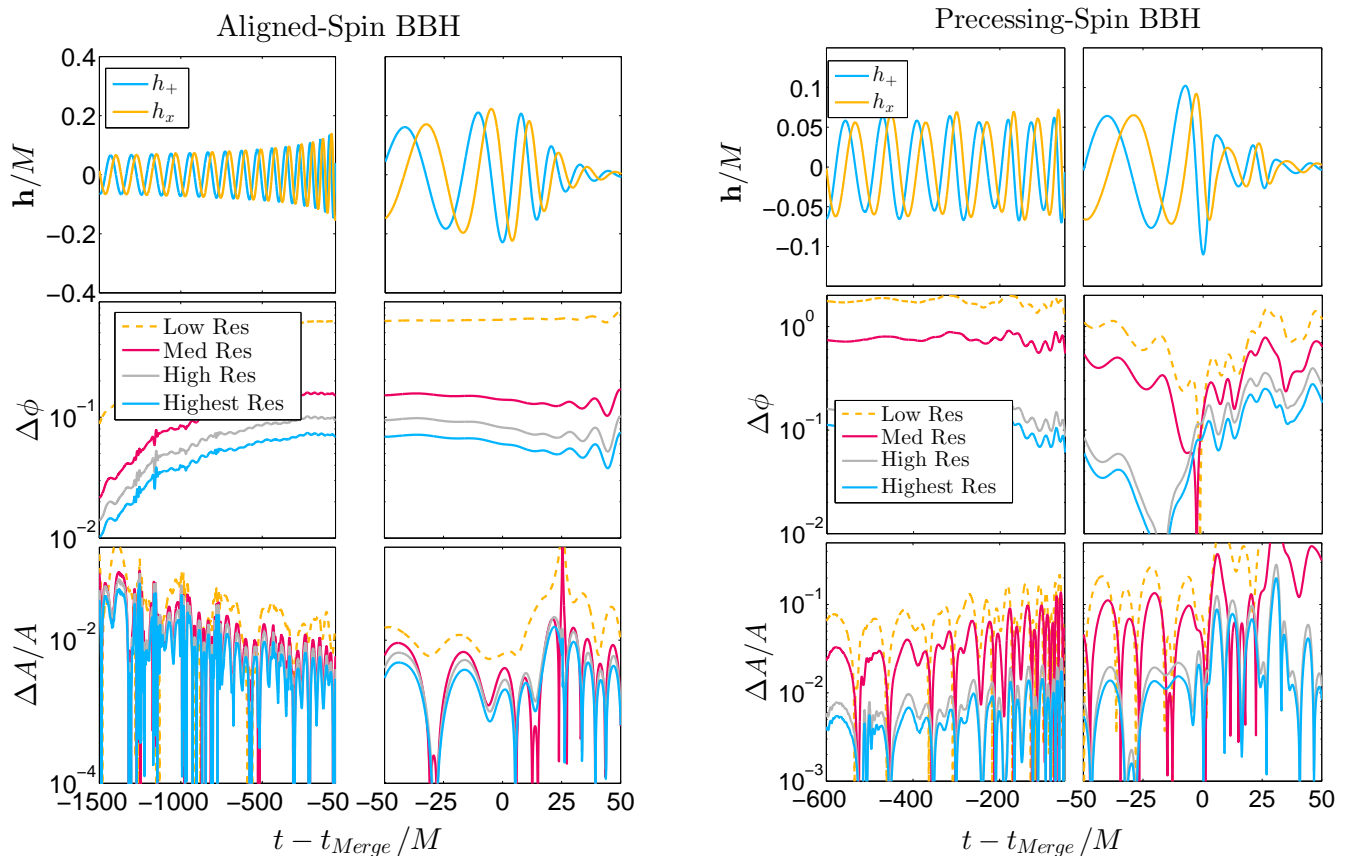


FIG. 2: Numerical errors in the amplitude and phase of the GW strain,  $h(t)$ , for  $\ell = 2 : 6, m = -\ell : \ell$  radiated modes. Left panels show results for the GT0582 case and right panels for the GT0560. Top panels depicts the strain  $h(t)$  at face-on location from detector. The middle and bottom panel shows the errors in phase and amplitude, respectively.

BBH Type	Mismatches from:		Errors in GW-strain:			
	Finite Resolution	Finite Extraction	$ \Delta A/A _{\text{Ins}}$	$\Delta\phi _{\text{Ins}}$	$\Delta A/A _{\text{Ref}}$	$\Delta\phi _{\text{Ref}}$
Aligned-Spin	$3.4 \times 10^{-6}$	$5.4 \times 10^{-5}$	$5.8 \times 10^{-4}$	$1.0 \times 10^{-2}$	$3.7 \times 10^{-2}$	$6.8 \times 10^{-2}$
Precessing-Spin	$4.0 \times 10^{-4}$	$4.7 \times 10^{-4}$	$3.6 \times 10^{-3}$	$1.1 \times 10^{-1}$	$1.2 \times 10^{-3}$	$2.6 \times 10^{-2}$

TABLE I: Typical numerical errors in GW strain for GT catalog. The numbers refer to the waveforms showcased in fig. 2.

### III. DESCRIPTION OF THE CATALOG

The initial data for each simulation in the catalog are fully characterized by a set of 15 parameters, as described in § II: BH masses  $m_1, m_2$ , spins  $\vec{\chi}_1, \vec{\chi}_2$ , momenta  $\vec{P}_1, \vec{P}_2$ , and the binary separation  $r$ . We select code units such that  $M = m_1 + m_2 = 1$ . The waveforms are classified into two main types: *Non-precessing* and *Precessing*. Non-precessing waveforms are subdivided into two sub-types: *Non-spinning* if the BHs in the binary are not spinning, and *Aligned-Spin* if their spins are parallel with the orbital angular momentum  $\vec{L}$  (spins of black hole that are anti-aligned and parallel to  $\vec{L}$  are put under the class of aligned-spin). The precessing waveforms are also subdivided into two sub-types: *Equal Mass* and *Unequal Mass*. Table II summarizes this classification.

The catalog can be found at [einstein.gatech.edu/catalog](http://einstein.gatech.edu/catalog). Each of the 452 waveforms in the catalog have a unique identifier of the form GTXXXX. The catalog is organized by folders. Each folder contains the following information:

- Initial parameters of BBH system
- Parameter file of the simulation
- BH trajectories
- Mass, spin and gravitational recoil of the final BH
- Radiated energy, linear momentum and angular momentum
- $\Psi_4$  decomposed in spin-weighted spherical harmonics with  $\ell \leq 8$  and different extraction radii

- The waveforms are available in HDF5 format with meta-data as stated in Ref. [32, 33].

Fig 1 provides a general sense of the parameter space covered by the catalog. The vertical axis in both plots denotes the mass ratio  $q$ . The plot in the left is for non-spinning and aligned-spin systems. Therefore, the axis in the plane are given in terms of  $\vec{\chi}_{1,2} \cdot \hat{L}$  in order to capture both the spin magnitude and orientation for each BH. The plot on the right in Fig. 1 describes the precessing runs. The axis in the plane are given in this case in terms of the  $\hat{\chi}_{1,2} \cdot \hat{L}$ , namely the spin orientation relative to the orbital angular momentum.

The scatter plot in Fig. 3 shows  $|\vec{\chi}_F|$ , the magnitude of the spin of the final BH, as a function of the percentage of total mass radiated, i.e.  $(1 - M_F/M) \times 100\%$ . Notice that binary systems with high final BH spin radiate the most energy. On the other hand, configurations that leave behind a slowly rotating BH radiated very little.

Type	Sub-type	Simulations
Non-Precessing	Non-Spinning	49
	Aligned-Spins	79
Precessing	Equal-Mass ( $q = 1$ )	127
	Unequal-Mass ( $q \neq 1$ )	197

TABLE II: GT catalog waveform classification

The histogram in Fig. 4 show the distribution  $M\omega_{\text{orb}}$

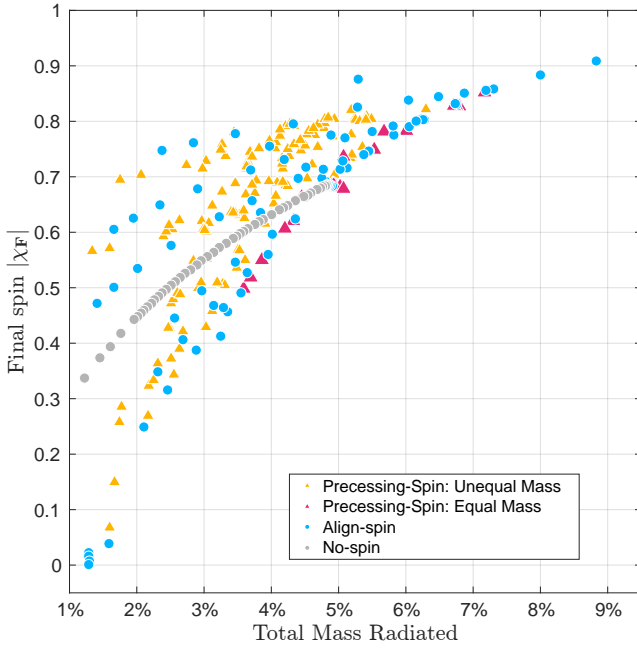


FIG. 3: Magnitude of the spin of the final BH  $|\vec{\chi}_F|$  as a function of the percentage of total mass radiated, i.e.  $(1 - M_F/M) \times 100\%$

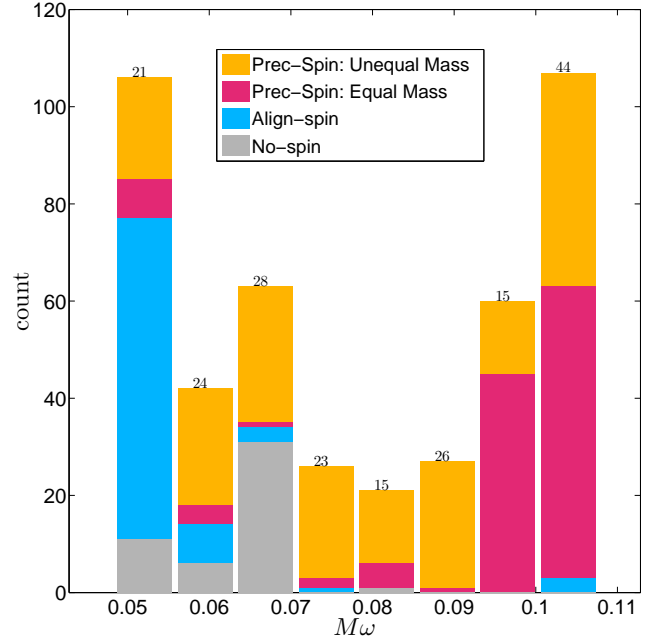


FIG. 4: The histogram showing the distribution of the  $M\omega_{\text{orb}}$ . For Advanced LIGO, the x-axis limit scales to  $[50, 110] M_\odot$  as range of minimum total mass  $M$ . The numbers on the top of each bar corresponds to the total unequal-mass precessing simulations in the stated range.

where  $\omega_{\text{orb}}$  the orbital frequency (half of gravitational-wave frequency). The NR waveforms presented the catalog include the early phase of the simulation that is contaminated with the junk radiation in the initial data. The segment of the waveform with orbital frequencies  $\leq M\omega_{\text{orb}}$  should hence be ignored. For a given low-frequency cutoff of a GW detector,  $f_{\text{min}}$ , the waveform can be scaled to a minimum total mass as  $M = k (M\omega_{\text{orb}}/f_{\text{min}})$ , where  $k = 3.23 \times 10^4$ . From Fig. 4 it can be inferred the catalog includes a large number of waveforms with less than four GW cycles. These are basically BBH plunges. They are nonetheless useful for studies of quasinormal ringing and gravitational recoil. Waveforms with between five to ten GW cycles are suitable to investigate BBH with massive BH such as GW150914.

Some of the highlights in the catalog are: The largest mass-ratio is  $q = 15$  for a non-spinning BBH (GT0601), while for precessing BBH  $q = 8$  (GT0886). The maximum spin for the merging BH is  $|\chi_{1,2}| = 0.8$ . The most extreme spin for the remnant BH is  $|\chi_F| = 0.9048$ , corresponding to 8.826% of the total-mass  $M$  radiated in GWs (GT0424) (see Fig. 3). The maximum total angular momentum radiated is  $\sim 100\%$  for a system of align-spin BBH which results in Schwarzschild-like remnant BH (GT0770). The maximum GW cycles in our simulation corresponds to 27.5 for align-spin (GT0612) and 21.5 for precessing-spin systems (GT0468).

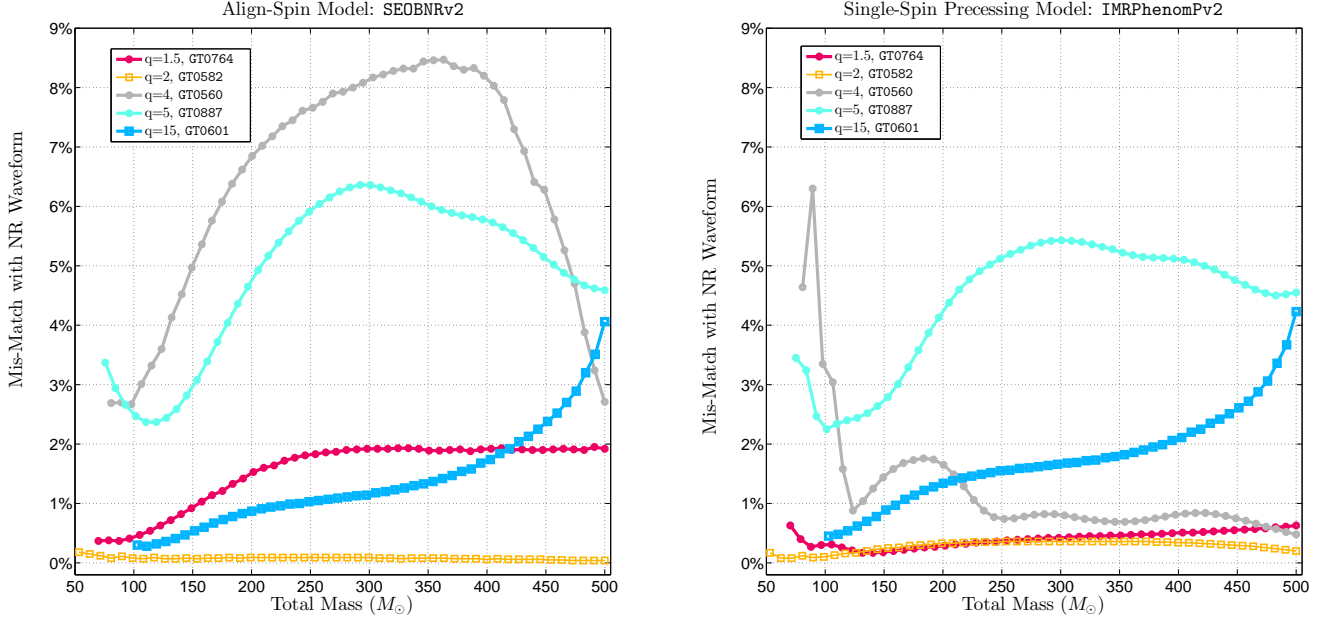


FIG. 5: Mismatches of NR waveforms in Table III with approximant GW models.

#### IV. COMPARISON WITH APPROXIMANT GRAVITATIONAL-WAVEFORM MODELS

Next we compare a few of the waveforms in the catalog with two recent and well-known approximate waveforms. The binary parameters of the selected waveforms are given in Table III, and the corresponding strains  $h(t)$  for the two cases ((GT0582 and GT0560) are shown in Fig. 2. The cases were chosen to probe highly distinct regions of parameter space.

The two approximate waveform models we use to compare our NR waveforms are: i) a time-domain model for non-precessing, aligned-spin systems, derived from the effective-one-body formalism (referred to as SEOBNRv2 [34, 35]) and ii) a phenomenological frequency-domain model for single-spin, precessing systems (referred to as IMRPhenomPv2 [36–38]). Both of these approximate models were used in the detection and parameter-estimation analysis of GW150914.

For each waveform in Table III, we compute their mismatch with both SEOBNRv2 and IMRPhenomPv2, where the mismatch is given by

$$\text{mismatch} = 1 - \max_{t_0, \phi_0} \frac{(h_1|h_2)}{\sqrt{(h_1|h_1)(h_2|h_2)}}, \quad (2)$$

where the inner product is given by

$$(h_1|h_2) = 4\text{Re} \int_{f_{\min}}^{\infty} \frac{\tilde{h}_1(f)\tilde{h}_2^*(f)}{S_h(f)} df. \quad (3)$$

The maximization in the mismatch (2) is over the initial arrival time and phase. In Eq. (3),  $S_h(f)$  is the

noise spectral density of the detector, and asterisks denote complex conjugation. The integral is evaluated from some minimum frequency  $f_{\min}$ , below which there is no appreciable contribution to the integrand due to the noise spectrum. We set as low-frequency cutoff  $f_{\min} = 30$  Hz and use a noise spectrum representative of advanced LIGO in its early configuration. To evaluate mismatch, both the waveforms, NR and the approximant models, are projected to the same optimal sky-location and orientation.

Figure 5 shows the mismatches for the NR waveforms in Table III with SEOBNRv2 and IMRPhenomPv2. The mismatch is computed for different values of total mass of BBH systems, starting from BBH systems with mass similar to GW150914 to intermediate mass BBH range for current generation of GW detectors. The NR waveform includes all the higher harmonics (as stated in eq. 1) from  $\ell = 2$  to 6; however, the approximant waveform includes only radiated mode  $\ell = 2, m = 2$ , which will be dominant for the chosen optimal sky-location and orientation.

ID	Type	$q$	$\vec{\chi}_1$	$\vec{\chi}_2$
GT0764	prec-spin	1.5	(0.6,0,0)	(0,0,0.6)
GT0582	aligned-spin	2	(0,0,-0.15)	(0,0,0.6)
GT0560	prec-spin	4	(-0.6,0,0)	(-0.6,0,0)
GT0887	prec-spin	5	(0.42, 0, 0.42)	(-0.42, 0, -0.42)
GT0601	non-spin	15	(0,0,0)	(0,0,0)

TABLE III: GT BBH simulations used for comparison with approximate GW models. The results are shown in fig. 5.



For the aligned spins with low-mass ratio, both models have a very strong agreement with NR waveform. For the non-spinning BBH with mass-ratio of  $q = 15$ , which represents an astrophysical intermediate-mass ratio inspiral BBH system, both **SEOBNRv2** and **IMRPhenomPv2** have a growing mismatch at high total mass. For such high masses, the signal in LIGO will be dominated by the merger and ringdown of BBH, and radiated modes beyond the dominant becomes important [39, 40]. Both the models only includes the dominant modes (2,2) and thus there is strong mismatch, even at optimal sky-location.

For the precessing-spin BBH systems, it is expected that **SEOBNRv2** will show strong inconsistency with NR simulations as the model is tuned only for aligned-spin systems. The max mismatch we report for **SEOBNRv2** in precessing cases, which happens for a system with mass-ratio  $q = 4$ . In contrast, for the same NR simulation (GT0560), the precessing spin model **IMRPhenomPv2** - reports an error up to 6% for lower total mass and drops to less than 1% at higher total mass. Both models agree fairly well with NR simulations for almost equal-mass systems, but for strongly deviate for mass-ratios  $q = 5$  and above (where higher radiated modes become important).

## V. MASS AND SPIN OF THE FINAL BH AND PHENOMENOLOGICAL FITS

As mentioned before, included in the GT catalog is information regarding the mass and spin of the final BH. Over the years, several phenomenological formulas have been proposed that connect the properties (mass and spin) of the remnant BH with the initial parameters of the BHs in the binary. In this section, we concentrate on two of such phenomenological formulas: one from Healy et al. [14], referred as RIT, and the other from Barausse et al. [13], referred as BR.

In Figure 6, we report the errors the phenomenological formulas incur in predicting the mass and spin of the final BH. The percentage errors are organized according to the sub-types in Table II, and they were calculated as  $(1 - \text{RIT or BR}/\text{NR}) \times 100\%$ . Top panels show the errors in the final mass and the bottom for the final spin. The red line in each box is the median value of the errors. On each box, the colored region denotes 75% of the cases. Notice that, for aligned-spin systems, the spread in errors for the remaining 25% cases (i.e. cases with the largest errors) is quite significant for both formulas. The RIT, valid for non-spinning and align-spinning BBH systems, has an average discrepancy with our catalog of 0.035% for the remnant mass and 0.23% for the remnant spin. The BR formula, valid for all generic BBH configurations, agrees remarkably with all our GT-BBH simulations, and with an average discrepancy of 0.6% for the final mass and 1.6% for the final spin. A recent paper by the authors [41] improves the BR formula for stronger agreements with generic BBH NR simulations.

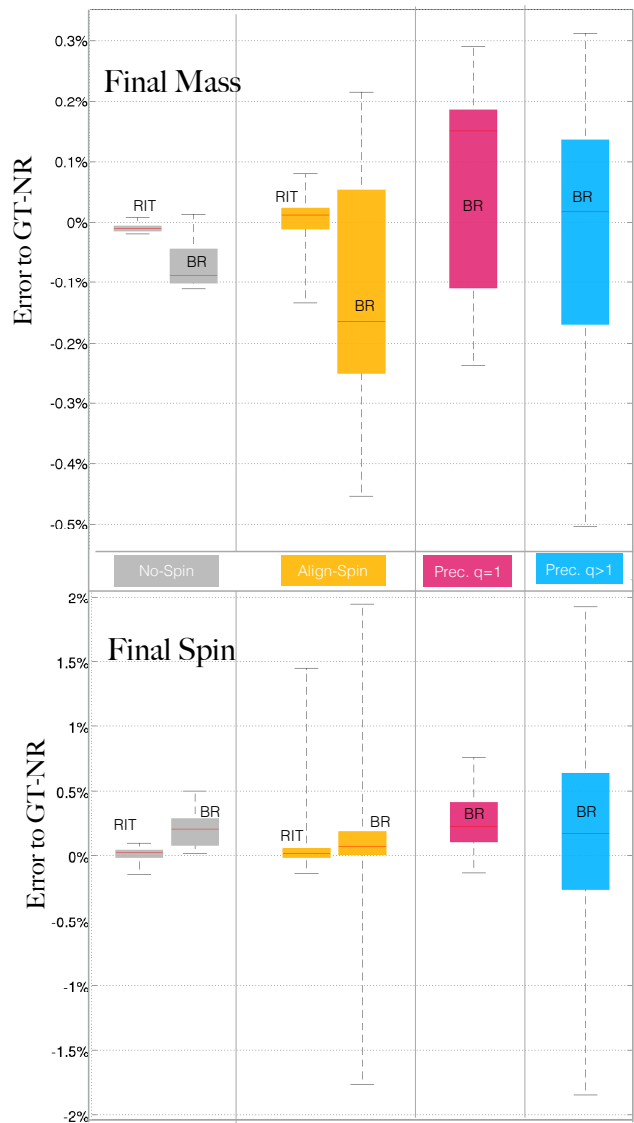


FIG. 6: Percentage relative errors predicting the mass and spin of the final BH from the RIT and BR fitting formulas when applied to our catalog. The red line in each box is the median value of the errors. The colored region within each box denote the 25 – 75 percentile of relative error in each case.

## VI. CONCLUSION

This paper introduced the GT catalog of GW waveforms consisting of 452 distinct waveforms from more than 600 spin-aligned and precessing BBH simulations with mass ratios of up to  $q = 15$ . The waveforms expand a moderate number of orbits in the late inspiral, the burst during coalescence, and the ring-down of the final black hole. A significant fraction of the waveforms have enough GW cycles that can be used in improving phenomenological or EOB models. The waveforms are also useful for tuning the phenomenological formulas describing the remnant black hole. Most of the waveforms

can be used directly in connection with analysis of massive BBH binaries such as GW150914 and for conducting tests of general relativity that require knowledge of both the inspiral and ringdown stages. The GT catalog complements and enhances the catalog recently introduced by the SXS collaborations [42]. The GT catalog contains waveforms of the higher modes and will serve as repository of future waveforms, including those from double neutron star and mixed binary mergers.

## Acknowledgments:

We would like to thank Juan Calderon Bustillo and Sebastian Khan for useful discussions. This work is supported by NSF grants 1505824, 1333360, and XSEDE TG-PHY120016.

- 
- [1] B. P. Abbott, R. Abbott, T. D. Abbott, M. R. Abernathy, F. Acernese, K. Ackley, C. Adams, T. Adams, P. Addesso, R. X. Adhikari, et al., *Physical Review Letters* **116**, 061102 (2016), 1602.03837.
  - [2] G. M. Harry (LIGO Scientific Collaboration), *Class. Quant. Grav.* **27**, 084006 (2010).
  - [3] The LIGO Scientific Collaboration and the Virgo Collaboration, *ArXiv e-prints* (2016), 1602.03840.
  - [4] The LIGO Scientific Collaboration and the Virgo Collaboration, *ArXiv e-prints* (2016), 1602.03841.
  - [5] The LIGO Scientific Collaboration and the Virgo Collaboration, *ArXiv e-prints* (2016), 1602.03843.
  - [6] B. Abbott and the LIGO Scientific Collaborations (LIGO Scientific Collaboration), *Physical Review D* **72**, 082001 (2005).
  - [7] B. Abbott and the LIGO Scientific Collaboration (LIGO Scientific Collaboration), *Physical Review D* **73**, 062001 (2006).
  - [8] The LIGO Scientific Collaboration, *Physical Review D* **77**, 062002 (2008), 0704.3368.
  - [9] The LIGO Scientific Collaboration, *Physical Review D* **78**, 042002 (2008), 0712.2050.
  - [10] Y. Pan, A. Buonanno, L. T. Buchman, T. Chu, L. E. Kidder, H. P. Pfeiffer, and M. A. Scheel, *Phys. Rev. D* **81**, 084041 (2010), URL <http://link.aps.org/doi/10.1103/PhysRevD.81.084041>.
  - [11] P. Ajith, M. Hannam, S. Husa, Y. Chen, B. Bruegmann, et al., *Phys. Rev. Lett.* **106**, 241101 (2011).
  - [12] E. Barausse and L. Rezzolla, *Astrophys.J.* **704**, L40 (2009), 0904.2577.
  - [13] E. Barausse, V. Morozova, and L. Rezzolla, *Astrophys.J.* **758**, 63 (2012), 1206.3803.
  - [14] J. Healy, C. O. Lousto, and Y. Zlochower, *Phys.Rev.* **D90**, 104004 (2014), 1406.7295.
  - [15] F. Herrmann, D. Shoemaker, and P. Laguna (2006), *gr-qc/0601026*.
  - [16] B. Vaishnav, I. Hinder, F. Herrmann, and D. Shoemaker, *Phys.Rev.* **D76**, 084020 (2007), 0705.3829.
  - [17] J. Healy, J. Levin, and D. Shoemaker, *Phys. Rev. Lett.* **103**, 131101 (2009).
  - [18] L. Pekowsky, R. OShaughnessy, J. Healy, and D. Shoemaker, *Phys.Rev.* **D88**, 024040 (2013), 1304.3176.
  - [19] T. W. Baumgarte and S. L. Shapiro, *Phys. Rev. D* **59**, 024007 (1999), *gr-qc/9810065*.
  - [20] M. Campanelli, C. O. Lousto, P. Marronetti, and Y. Zlochower, *Phys. Rev. Lett.* **96**, 111101 (2006).
  - [21] J. G. Baker, J. Centrella, D.-I. Choi, M. Koppitz, and J. van Meter, *Phys.Rev.Lett.* **96**, 111102 (2006), *gr-qc/0511103*.
  - [22] et-web, einstein Toolkit home page:<http://www.einsteintoolkit.org>.
  - [23] G. Allen, T. Goodale, and E. Seidel, in *7th Symposium on the Frontiers of Massively Parallel Computation-Frontiers 99* (IEEE, New York, 1999).
  - [24] E. Schnetter, S. H. Hawley, and I. Hawke, *Class. Quant. Grav.* **21**, 1465 (2004).
  - [25] S. Husa, I. Hinder, and C. Lechner, *Computer Physics Communications* **174**, 983 (2006).
  - [26] J. M. Bowen and J. W. York, Jr., *Phys. Rev. D* **21**, 2047 (1980).
  - [27] M. Ansorg, B. Brügmann, and W. Tichy, *Phys. Rev. D* **70**, 064011 (2004), *gr-qc/0404056*.
  - [28] S. Husa, M. Hannam, J. A. González, U. Sperhake, and B. Brügmann, *Phys. Rev. D* **77**, 044037 (2008), 0706.0904.
  - [29] W. Tichy and P. Marronetti, *Phys. Rev. D* **83**, 024012 (2011), 1010.2936.
  - [30] C. Reisswig, N. T. Bishop, D. Pollney, and B. Szilagyi, (*arXiv:0912.1285*) (2009), URL <http://xxx.lanl.gov/abs/arXiv:0912.1285>.
  - [31] I. Hinder et al., *Class. Quant. Grav.* **31**, 025012 (2014), 1307.5307.
  - [32] P. Schmidt, I. W. Harry, and H. P. Pfeiffer, *In Prep* (2016).
  - [33] C. R. Galley and P. Schmidt, *In Prep* (2016).
  - [34] A. Taracchini et al., *Phys. Rev.* **D89**, 061502 (2014), 1311.2544.
  - [35] M. Pürrer, *Phys. Rev. D* **93**, 064041 (2016), URL <http://link.aps.org/doi/10.1103/PhysRevD.93.064041>.
  - [36] S. Khan, S. Husa, M. Hannam, F. Ohme, M. Pürrer, X. J. Forteza, and A. Bohé, *Phys. Rev. D* **93**, 044007 (2016), URL <http://link.aps.org/doi/10.1103/PhysRevD.93.044007>.
  - [37] P. Schmidt, M. Hannam, and S. Husa, *Phys. Rev.* **D86**, 104063 (2012), 1207.3088.
  - [38] M. Hannam, P. Schmidt, A. Bohé, L. Haegel, S. Husa, F. Ohme, G. Pratten, and M. Pürrer, *Phys. Rev. Lett.* **113**, 151101 (2014), URL <http://link.aps.org/doi/10.1103/PhysRevLett.113.151101>.
  - [39] J. Caldern Bustillo, S. Husa, A. M. Sintes, and M. Prerrer, *Phys. Rev.* **D93**, 084019 (2016), 1511.02060.
  - [40] L. London, J. Healy, and D. Shoemaker (2014), 1404.3197.
  - [41] F. Hofmann, E. Barausse, and L. Rezzolla (2016), 1605.01938.
  - [42] A. H. Mroué, M. A. Scheel, B. Szilágyi, H. P. Pfeiffer, M. Boyle, D. A. Hemberger, L. E. Kidder, G. Lovelace, S. Ossokine, N. W. Taylor, et al., *Physical Review Letters*

111, 241104 (2013), 1304.6077.